applied sciences

MDPI

Article

Electrical and Mechanical Properties of Ink Printed Composite Electrodes on Plastic Substrates

Xinda Wang [1], Wei Guo [1], Ying Zhu [1], Xiaokang Liang [2], Fude Wang [2] and Peng Peng [1,3,*]

1 School of Mechanical Engineering and Automation, Beihang University, Beijing 100191, China; wxd8166@163.com (X.W.); gwei@buaa.edu.cn (W.G.); bh_zhuying@buaa.edu.cn (Y.Z.)
2 Capital Aerospace Machinery Co., Ltd., Beijing 100076, China; camc_liangxk@163.com (X.L.); wangfude66@hotmail.com (F.W.)
3 International Research Institute for Multidisciplinary Science, Beihang University, Beijing 100191, China
* Correspondence: ppeng@buaa.edu.cn; Tel.: +86-10-8231-7712

Received: 26 September 2018; Accepted: 26 October 2018; Published: 1 November 2018

Featured Application: This study focuses on fabricating of flexible composite electrodes with low electrical resistance and good mechanical performance at a low temperature by introducing the second phase of fillers with different dimensions.

Abstract: Printed flexible electrodes with conductive inks have attracted much attention in wearable electronics, flexible displays, radio-frequency identification, etc. Conventional conductive inks contain large amount of polymer which would increase the electrical resistivity of as-printed electrodes and require high sintering temperature. Here, composite electrodes without cracks were printed on polyimide substrate using binder-free silver nanoparticle based inks with zero-dimensional (activated carbon), one-dimensional (silver nanowire and carbon nanotube) or two-dimensional (graphene) fillers. The effect of fillers on resistivity and flexibility of printed composite electrodes were evaluated. The graphene filler could reduce the resistivity of electrodes, reaching 1.7×10^{-7} Ω·m after low power laser sintering, while the silver nanowire filler improved their flexibility largely during bending tests. The microstructural changes were examined to understand the nanojoining process and their properties.

Keywords: ink printing; nanojoining; laser sintering; mechanical performance

1. Introduction

Printed flexible electrodes have attracted great attention in a variety of newly emerging areas such as printable transistors, flexible displays, electrodes, sensors, antennas, radio-frequency identification tags, solar cells, etc. [1]. Currently, inkjet [2], screen [3], gravure [4] and aerosol printing [5] techniques can be used to print desired patterns on flexible substrates, such as polyimide, polyethylene terephthalate and polycarbonate. During printing, conductive inks are essential, associating with the feasibility of electrode deposition, bonding at electrode–substrate interface, offering conductivity, etc., which usually contain highly conductive materials, such as silver, gold, carbon nanotubes or graphene, binders, solvents and other fillers [6], to adjust their physicochemical properties. Among them, the used binders are typically polymers, such as acrylics [7], alkyds [8], cellulose [9] and rubber resins [10]. Although these binders can connect conductive filler elements to each other and offer good formability during printing, they also bring insufficient electrical conductivity due to their non-conductivity. Further, the presence of such binders complicates the curing and sintering processes because longer time or higher temperature is needed to remove or decompose them [11]. In traditional thermal sintering, a high temperature is needed to decompose this organic content and promote atomic

interdiffusion to form a metallic bond between metallic fillers [12]. However, flexible substrates usually cannot withstand such high temperature [13]. Therefore, sintering temperature is particularly important when heat sensitive substrates are involved, making low-temperature sintering essential to avoid mechanical or thermal degradation of the substrate [14]. This requires reduced organic content in conductive inks. Besides that, the two prevalent droplet jetting mechanisms for inkjet printing, continuous inkjet and drop-on-demand inkjet, require low viscosity inks, which are beneficial to stable jetting and suppression of generation of satellite droplets [15]. The addition of binders will significantly increase the viscosity of inks [11].

In recent years, there has been increasing interests given to binder-free conductive inks. Hu et al. [16] demonstrated a binder-free, stable black phosphorus ink formulation using a mixture of IPA/2-butanol solvents. The low surface tension ensured wetting of a variety of untreated substrates, enabling good consistency and spatially uniform. Printable radio frequency identification antenna with ultra-low resistance was achieved by binder-free graphene laminate [17]. The conductivity of graphene laminate is improved by more than 50 times with rolling compression, reaching 4.3×10^4 S/m, almost double the 2.5×10^4 S/m of previously reported graphene laminate with binder. Referring to electronic industry, silver inks with heavy binder content are widely used. To increase the electrical performance and mechanical reliability of printed electrodes, adding the second phase of filler materials for inkjet printing was reported. For example, Hoeng et al. [18] proposed that adding cellulose nanocrystals into silver ink can improve electrical conductivity and mechanical performance of printed films, providing a new solution to obtain conductive patterns on a porous substrate with a low sheet resistance of 50 Ω/sq. Joo et al. [19] demonstrated a composite copper nanoparticle based ink with 5 wt.% copper nanowires filler can reach a resistivity of 2.3×10^{-7} Ω·m for electrodes compared with 9.4×10^{-7} Ω·m for those printed by pure copper nanoparticle inks. However, if binders are removed, the silver particles have difficulty forming a continuous track without linkages by binders, leading to cracking of printed structure [20], large interface resistance [17] and less mechanical reliability [21].

To investigate the feasibility of printing silver based flexible electrodes using binder-free inks, in this study, silver nanoparticles (Ag NPs), binary solvents, and conductive nanofillers with zero-, one-, and two-dimensions were used to fabricate binder-free inks. Appearance, microstructure, electrical resistivity and bending performance of printed electrodes on polyimide (PI) substrate were evaluated. Laser sintering was also used to increase joining between conductive fillers to enhance their conductivity.

2. Materials and Methods

2.1. Materials

Analytical reagents including silver nitrate ($AgNO_3$), glucose, Polyvinyl Pyrrolidone (PVP, K30, $M_w \approx 40{,}000$ g·mol^{-1}), sodium hydroxide (NaOH), ethylene glycol (EG), and trition X-100 (TX-100) were purchased from Aladdin Industrial Corporation. Activated carbon (AC, 99.9%, Ningbo Jin Lei Nano Mstar Technology Ltd., Ningbo, China), multi wall carbon nanotubes (CNT, Shenzhen Nanotech Port Co., Ltd., Shenzhen, China), graphene (G, The Sixth Element Materials Technology Co., Ltd., Changzhou, China), and silver nanowires (Ag NW, synthesized in the lab) were used as the second phase of conductive fillers. Ag NPs were synthesized using a modified procedure from the literature [22]. In general, the mixture of 30 mL $AgNO_3$ aqueous solution (5.1 g $AgNO_3$) with 200 mL glucose (14 g) and PVP (8 g) aqueous solution was heated to 90 °C for 30 min under vigorous stirring, and then naturally cooled. The product was ultrasonicated, centrifuged, and dried at 50 °C. The synthesized Ag NPs were coated with a PVP shell, which can effectively prevent the agglomeration of Ag NPs. Ag nanowires were synthesized with polyol method [23]. The dimensions of fillers are shown in Table 1.

Table 1. The dimensions of fillers.

Filler	Dimension
AC(0D)	Amorphous form
AgNP(0D)	Average diameter: 40 nm,
CNT(1D)	Average diameter: 30 nm, Length: less than 2 μm
AgNW(1D)	Average diameter: 75 nm, Length: less than 5 μm
G(2D)	Average width: 10 μm

2.2. Preparation of Composite Inks

Table 2 lists the ink composition. The pure Ag NP ink served as a control sample for comparison. Zero-dimensional activated carbon (AC), one-dimensional silver nanowires (Ag NWs) and carbon nanotubes (CNTs) and two-dimensional graphene (G) were added into pure Ag NP ink with a concentration below their percolation threshold [24–27]. The solvent contained water and ethylene glycol with a volume ratio of 3:1. To ensure uniform dispersion of inks, trace surfactant (0.1 wt.% TX-100) was used in inks.

Table 2. Contents of composite inks.

Sample	Filler (30 wt.%)	Solvent (69.9 wt.%)		Surfactant (0.1 wt.%)
Pure Ag NP	Ag NP	H_2O	EG	TX-100
Ag NP/AC	29.7%Ag NP, 0.3%AC	H_2O	EG	TX-100
Ag NP/Ag NW	24%Ag NP, 6%Ag NW	H_2O	EG	TX-100
Ag NP/CNT	29.7%Ag NP, 0.3%CNT	H_2O	EG	TX-100
Ag NP/G	29.7%Ag NP, 0.3%G	H_2O	EG	TX-100

2.3. Inkjet Printing of Composite Electrodes and Low Temperature Sintering

The PI film with thickness of 0.3 mm served as substrate. Five types of inks were printed using an inkjet printer (Microplotter proto, Sonoplot, Middleton, WI, USA) with a capillary needle of 40 μm inner diameter and printing speeds of 1 mm/s. The binder-free and water-based inks led to quick drying process. Laser sintering was conducted by an 808 nm diode laser with a spot diameter of 500 μm. After the attenuation, the working power of the laser was 1.5 W with a constant power density of 7.6 W/mm^2.

2.4. Characterization

The microstructure, morphology and thickness were characterized by field emission scanning electron microscopy (FESEM, Merlin compact, Berlin, Germany). The four-point resistance of printed tracks was measured with a source meter (Keithley, 2400). The resistivity ϱ was calculated using ϱ = RS/L, where R is the measured four-point resistance, S is the cross-section area and L is the length of the electrodes. Resistivity of various forms of carbon fillers were measured by four-point method after pressing them into 10 mm × 10 mm × 1 mm pieces. The results show that AC, CNT and G have a resistivity of 10^{-2}, 10^{-4} and 10^{-7} Ω·m, respectively. The 20 mm electrodes were used for bending tests with a homemade bending device. Bending frequency was 15 cycles/min and bending degree was 50%, which is the ratio of the bended length to original electrode length.

3. Results and Discussion

The synthesized Ag NPs have an average diameter of 40 nm, and Ag NWs were 75 nm thick and less than 5 μm long, as shown in Figure 1. Five composite inks were printed onto clean PI substrate by multiple passes (five passes). The composite electrodes printed with the five inks on the surface presented continuous, uniform and crack-free morphologies (see Figure 2a). When the ink was ejected from the nozzle, it spread out on substrate due to its low viscosity and high surface

energy of PI (37 mN/m) [28], causing the line width of electrodes to be much larger than the original nozzle diameter (40 μm), but could deposit evenly on the substrate. These binder-free inks allow thin electrode deposition. When printed five times, the thickness of electrodes was less than 2.4 μm. Figure 2b shows the width and height of the as-printed composite electrodes. For example, Ag NP/AC electrode is 1.86 μm thick, as shown in inset image of Figure 2b.

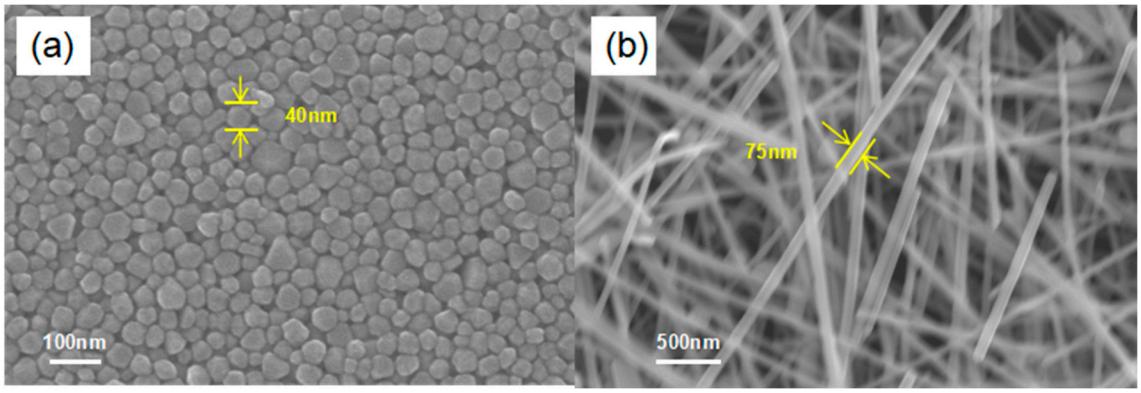

Figure 1. The morphology of synthesized silver: (**a**) nanoparticles; and (**b**) nanowires.

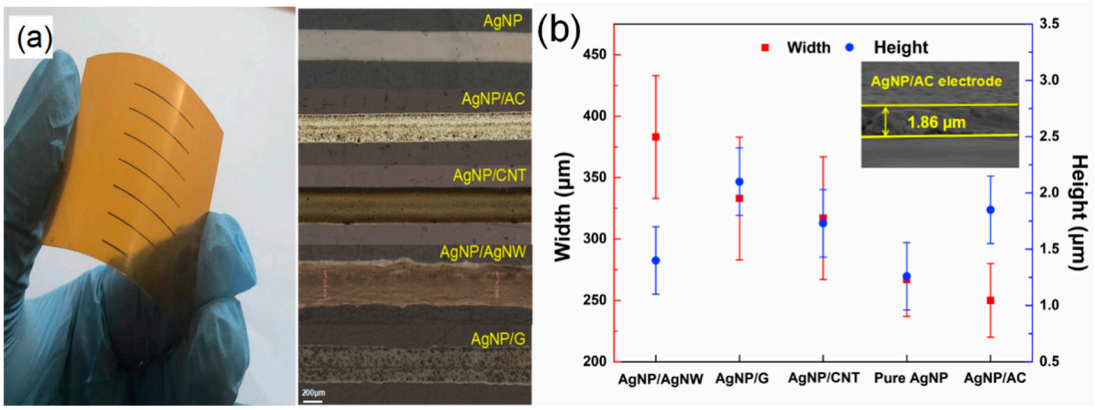

Figure 2. (**a**) Photograph and surface morphology of printed composite electrodes; and (**b**) thickness and line width of printed composite electrodes.

Since no binders was used in these inks, the as-printed electrodes could dry at low temperature (50 °C). After drying, they showed very large resistance as thin PVP shells presented on the surface of Ag NPs, and the interfaces of Ag NPs or between Ag NPs with added the second phase of filler materials formed interconnections for electrons to pass through [29]. To increase its conductivity, laser sintering was used due to its high efficiency and selectivity in area [30]. In addition, it can significantly reduce the input heat and minimize thermal damage to PI substrates. Figure 3 shows a schematic of laser sintering process. When laser irradiates the nanoparticles, the effect of surface plasmonic triggers Ag NPs to convert light into heat [31]. This photothermal effect firstly resulted in the fracture of C-O-Ag bond between Ag NPs and PVP [32]. Consequently, it induced desorption or decomposition of the PVP layer of Ag NPs to leave a bare silver surface with high surface energy and high curvature for diffusion of surface atoms and nanoscopic interconnection [33]. In addition, plasmonic effect of silver caused by laser occurred at a small gap between two adjacent nanoparticles, making "hot spots" with high energy [34]. This concentration of light could induce a high temperature locally without heating the surroundings to minimize the heat damage to substrate as thermal sintering does [31,35]. With the help of hot spots, local high temperature promoted the diffusion of atoms to form neck between Ag NPs during laser sintering [36].

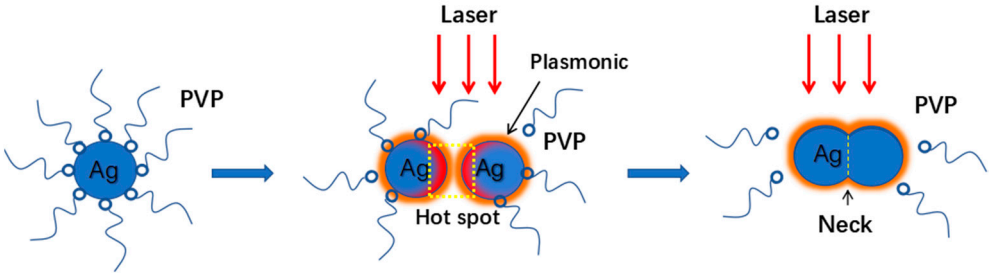

Figure 3. Schematic of laser sintering of PVP capped Ag NPs.

Figure 4 shows the curve of resistivity as a function of the laser scanning times. The resistivity decreases significantly with the first few repeated scans and eventually remained stable with further increasing scanning times, indicating laser sintering induced many interconnections between conductive filler materials quickly. Here, the second phase of filler can affect the resistivity of printed electrodes. The resistivity of Ag NP/G composite electrodes decreased from 2.8×10^{-7} to 1.7×10^{-7} Ω·m (10% of the conductivity of bulk silver), which is approximately 61% of the resistivity of pure Ag NP electrodes. During sintering process, diffusion between silver was much easier than carbon–carbon or carbon–silver due to their same crystal structure, atoms, and less activation energy [37]. Therefore, with the same dimensions, electrodes with silver fillers have a better conductivity than those with carbon. For example, the printed pure Ag NP electrodes had a lower resistivity (2.8×10^{-7} Ω·m) than Ag NP/AC composite electrodes (3.2×10^{-7} Ω·m). The results also show that the dimension of the fillers can influent their resistivity. It was found that a small amount of CNTs have the same effect in reducing resistivity as adding 6% Ag NWs in the ink. The resistivity of Ag NP/CNT composite electrodes is 2.0×10^{-7} Ω·m, which is close to that of Ag NP/Ag NW electrodes (2.1×10^{-7} Ω·m). However, they are higher than Ag NP/G composite electrodes with 2D fillers (1.7×10^{-7} Ω·m). These composite electrodes reach the same level of resistivity, 1.0×10^{-7} Ω·m, of Ag NP ink with a silver concentration of 50 wt.% [38].

The overall resistance of an electrical network comes from the bulk resistance of fillers, constriction resistance and tunneling resistance. The constriction resistance comes from the spots where there is direct contact between the conductive fillers and it increases with the number of contact points. The tunneling resistance comes from the spots where there is no direct connection between conductive fillers and, therefore, electrons need to overcome barrier energy to transfer through those spots [39]. When the concentration of filler is below the percolation threshold, the tunneling resistance will be a dominating factor compared with constriction resistance. To understand the contribution of the second phase fillers in the electrodes, SEM analysis (see Figure 5) was performed. Figure 5a shows the formation of bounds between particles, indicating the sintering of Ag NPs creates more interconnections for electron paths. However, the higher porosity results in a high tunnel resistance in the system. In Ag NP/CNT and Ag NP/Ag NW composite electrode systems, as schematically shown in Figure 5c,d, CNTs and Ag NWs can serve as bridges to connect Ag NPs. This bridging effects helping the development of more electrical paths and as a result convert the tunnel resistance into a lower contact resistance. As for 2D filler, as illustrated in Figure 5e, large graphene sheets can connect more Ag NPs because of their large surface area [40], resulting in more contact points and significantly decreased tunnel resistance, contributing to better conductivity. However, 0D material (AC) cannot bridge Ag NPs (see Figure 5b) which result in a high tunneling resistance. Meanwhile, due to a high bulk resistance of AC caused by many pore structures and destructed sp2 hybridization [41], Ag NP/AC composite electrodes displayed the highest resistivity. To verify the results, composite electrodes with 6 wt.% silver microflakes (average width of 600 nm) were sintered under the same laser parameters, and the results show that the composite electrodes exhibit the lowest resistivity of 1.1×10^{-7} Ω·m (Figure 4).

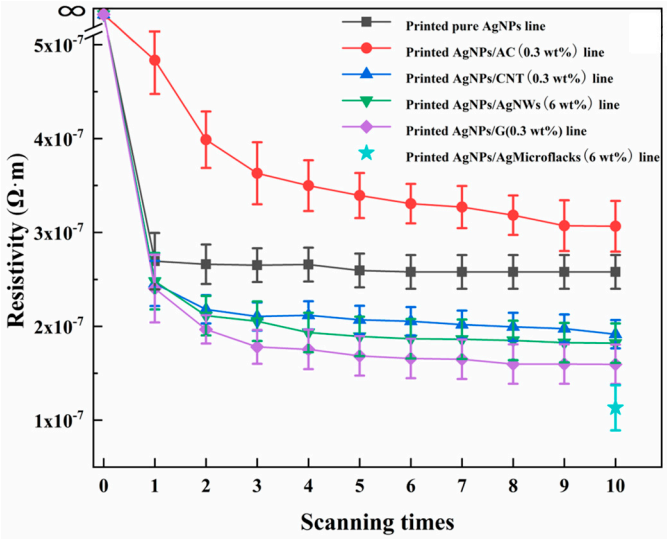

Figure 4. The resistivity as a function of laser scanning times.

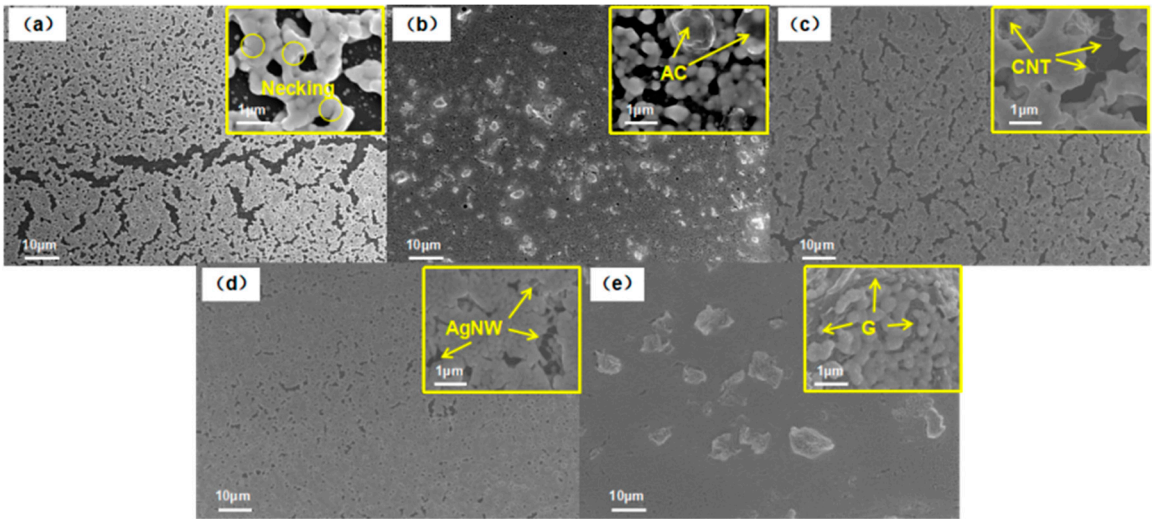

Figure 5. Scanning electron micrograph of sintered electrodes with: (**a**) AgNP; (**b**) AgNP/AC; (**c**) AgNP/CNT; (**d**) AgNP/AgNW; and (**e**) AgNP/G inks.

The flexibility of these as-printed and sintered composite electrodes was characterized. The rate of change of resistance in the electrodes is calculated using $K = (R - R_0)/R_0$, where R is the resistance of the electrodes after bending, and R_0 is that before bending. As shown in Figure 6, the bending properties of the electrodes also showed a strong correlation to the type and dimension of the second phase fillers. After 3000 bending cycles, the composite electrodes with AC, CNT and G fillers had a high K value, above 100%. However, the K value of pure Ag NPs and Ag NP/Ag NW electrodes were less than 20%. It suggests that the Ag electrodes can maintain their conductivity during deformation unlike the Ag/C electrodes (with AC, CNTs, or G). This is due to more interconnections and better interfacial strength for silver–silver than silver–carbon after sintering. In Ag NP/Ag NW electrodes, fillers were bonded through metallic bonds. However, the connections between carbon and silver were mainly by van der Waals bonds, which results in a lower interface bonding strength [42]. As shown in Figure 7a, in printed pure Ag NP electrode after bending test, Ag was still connected due to its good ductility. As for Ag NP/AC composite electrodes (Figure 7b), Ag debonded with AC to form isolated particles and reduced their interconnections. However, as 1D material, CNTs were pulled out from silver due to weak bonding between silver and carbon (Figure 7c), while some Ag NWs deformed plastically and some were still in bridging (Figure 7d). For Ag NP/carbon electrodes, Ag NP/G shows

highest K value after 3000 bending cycles, meaning bad flexibility. Figure 7e shows the microstructure of Ag NP/G electrodes after bending. During bending, graphene sheets could detach with silver and generate large microcracks due to the weak interfacial bonding and large stiffness mismatch between silver and graphene [43]. This study shows that electrical and mechanical properties can be tuned by adding different dimensional fillers in binder-free inks, which could benefit the ink formulation and ink-printing technique for electrode fabrication.

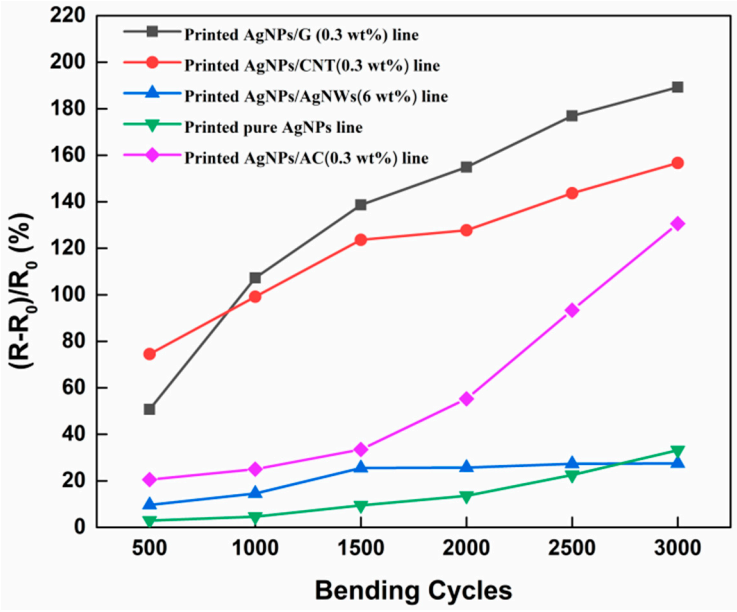

Figure 6. The change of resistance in composite electrode during bending.

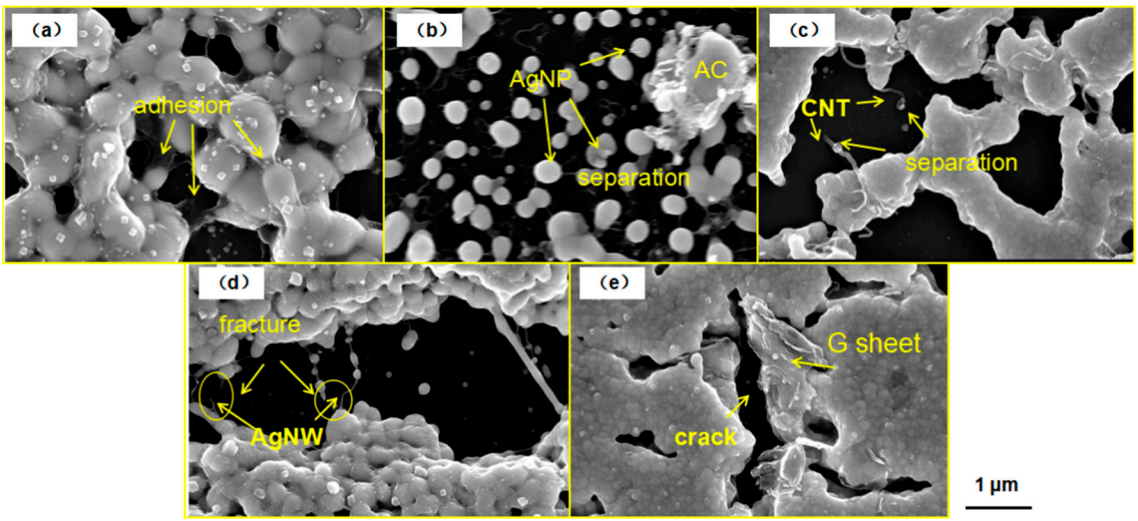

Figure 7. SEM images of composite electrodes with: (**a**) Ag NP; (**b**) Ag NP/AC; (**c**) Ag NP/CNT; (**d**) Ag NP/Ag NW; and (**e**) Ag NP/G fillers after bending test.

4. Conclusions

Binder-free silver nanoparticle based composite inks were utilized to fabricate flexible electrodes by ink printing. By adding the second phase of conductive fillers and using binary solvent, printed composite electrodes were uniform and without cracks. One dimensional fillers could serve as bridges in electrodes to enhance the conductivity and stability during bending. The graphene filler in composite electrodes could largely reduce average resistivity to 1.7×10^{-7} Ω·m after sintering but showed worse stability than adding Ag NWs, CNTs or AC. Ag NW filler in electrodes could lower

the resistance change less than 20% after 3000 bending cycles, indicating a good stability due to their bridging effect and strong interconnections with Ag NPs. These binder-free composite inks can be used for low temperature fabrication of flexible electrodes with low electrical resistance and good mechanical performance.

Author Contributions: X.W. and P.P. conceived and designed the experiments; X.W. performed the experiments; Y.Z., W.G., P.P. and X.W. analyzed the data; X.L. and F.W. contributed materials and analysis tools; and X.W. wrote the manuscript.

Funding: We acknowledge funding from the National Key R&D Program of China (2017YFB1104900), and the National Natural Science Foundation of China (No. 51605019).

Conflicts of Interest: The authors declare no conflicts of interest.

References

1. Abbel, R.; Teunissen, P.; Michels, J.; Groen, W.A. Narrow Conductive Structures with High Aspect Ratios Through Single-Pass Inkjet Printing and Evaporation-Induced Dewetting. *Adv. Eng. Mater.* **2015**, *17*, 615–619. [CrossRef]
2. Kim, C.; Nogi, M.; Suganuma, K.; Yamato, Y. Inkjet-printed lines with well-defined morphologies and low electrical resistance on repellent pore-structured polyimide films. *ACS Appl. Mater. Interfaces* **2012**, *4*, 2168–2173. [CrossRef] [PubMed]
3. Hoeng, F.; Denneulin, A.; Reverdy-Bruas, N.; Krosnicki, G.; Bras, J. Rheology of cellulose nanofibrils/silver nanowires suspension for the production of transparent and conductive electrodes by screen printing. *Appl. Surf. Sci.* **2017**, *394*, 160–168. [CrossRef]
4. Shiokawa, D.; Izumi, K.; Sugano, R.; Sekine, T.; Minami, T.; Kumaki, D.; Tokito, S. Development of a silver nanoparticle ink for fine line patterning using gravure offset printing. *Jpn. J. Appl. Phys.* **2017**, *56*, 05EA04. [CrossRef]
5. Zhao, D.; Liu, T.; Park, J.G.; Zhang, M.; Chen, J.-M.; Wang, B. Conductivity enhancement of aerosol-jet printed electronics by using silver nanoparticles ink with carbon nanotubes. *Microelectron. Eng.* **2012**, *96*, 71–75. [CrossRef]
6. Zhang, Y.; Li, X.; Mou, X.; Li, N. Preparation and Performance of Edible Screen-Printing Ink with Chitosan. In *Advanced Graphic Communications, Packaging Technology and Materials*; Springer: Singapore, 2016; pp. 977–983.
7. Zhang, J.; Li, X.; Shi, X.; Hua, M.; Zhou, X.; Wang, X. Synthesis of core–shell acrylic–polyurethane hybrid latex as binder of aqueous pigment inks for digital inkjet printing. *Prog. Natl. Sci. Mater. Int.* **2012**, *22*, 71–78. [CrossRef]
8. Tai, J.L.; Chen, G.X.; Chen, Q.F.; Tang, B.L. Study on Polyurethane-Acrylic Hybrid Emulsion Applying to Water-Based Ink. *Appl. Mech. Mater.* **2012**, *182–183*, 3–7. [CrossRef]
9. Dimic-Misic, K.; Gane, P.A.C.; Paltakari, J. Micro- and Nanofibrillated Cellulose as a Rheology Modifier Additive in CMC-Containing Pigment-Coating Formulations. *Ind. Eng. Chem. Res.* **2013**, *52*, 16066–16083. [CrossRef]
10. Lu, Z.; Jiang, X.; Zuo, X.; Feng, L. Improvement of cytocompatibility of 3D-printing resins for endothelial cell adhesion. *RSC Adv.* **2016**, *6*, 102381–102388. [CrossRef]
11. Hu, G.; Kang, J.; Ng, L.W.T.; Zhu, X.; Howe, R.C.T.; Jones, C.G.; Hersam, M.C.; Hasan, T. Functional inks and printing of two-dimensional materials. *Chem. Soc. Rev.* **2018**, *47*, 3265–3300. [CrossRef] [PubMed]
12. Peng, P.; Hu, A.; Zhou, Y. Laser sintering of silver nanoparticle thin films: Microstructure and optical properties. *Appl. Phys. A* **2012**, *108*, 685–691. [CrossRef]
13. Ko, S.H.; Pan, H.; Grigoropoulos, C.P.; Luscombe, C.K.; Fréchet, J.M.J.; Poulikakos, D. All-inkjet-printed flexible electronics fabrication on a polymer substrate by low-temperature high-resolution selective laser sintering of metal nanoparticles. *Nanotechnology* **2007**, *18*, 345202. [CrossRef]
14. Cheng, Y.-T.; Uang, R.-H.; Chiou, K.-C. Effect of PVP-coated silver nanoparticles using laser direct patterning process by photothermal effect. *Microelectron. Eng.* **2011**, *88*, 929–934. [CrossRef]
15. Derby, B. Inkjet Printing of Functional and Structural Materials: Fluid Property Requirements, Feature Stability, and Resolution. *Ann. Rev. Mater. Res.* **2010**, *40*, 395–414. [CrossRef]

16. Hu, G.; Albrow-Owen, T.; Jin, X.; Ali, A.; Hu, Y.; Howe, R.C.T.; Shehzad, K.; Yang, Z.; Zhu, X.; Woodward, R.I.; et al. Black phosphorus ink formulation for inkjet printing of optoelectronics and photonics. *Nat. Commun.* **2017**, *8*, 278. [CrossRef] [PubMed]
17. Huang, X.; Leng, T.; Zhang, X.; Chen, J.C.; Chang, K.H.; Geim, A.K.; Novoselov, K.S.; Hu, Z. Binder-free highly conductive graphene laminate for low cost printed radio frequency applications. *Appl. Phys. Lett.* **2015**, *106*, 203105. [CrossRef]
18. Hoeng, F.; Bras, J.; Gicquel, E.; Krosnicki, G.; Denneulin, A. Inkjet printing of nanocellulose–silver ink onto nanocellulose coated cardboard. *RSC Adv.* **2017**, *7*, 15372–15381. [CrossRef]
19. Joo, S.J.; Park, S.H.; Moon, C.J.; Kim, H.S. A highly reliable copper nanowire/nanoparticle ink pattern with high conductivity on flexible substrate prepared via a flash light-sintering technique. *ACS Appl. Mater. Interfaces* **2015**, *7*, 5674–5684. [CrossRef] [PubMed]
20. Sanchez-Romaguera, V.; Wünscher, S.; Turki, B.M.; Abbel, R.; Barbosa, S.; Tate, D.J.; Oyeka, D.; Batchelor, J.C.; Parker, E.A.; Schubert, U.S.; et al. Inkjet printed paper based frequency selective surfaces and skin mounted RFID tags: The interrelation between silver nanoparticle ink, paper substrate and low temperature sintering technique. *J. Mater. Chem. C* **2015**, *3*, 2132–2140. [CrossRef]
21. Li, J.; Fan, C.; Li, Q.; Wang, H.; Zhang, X. In situ studies on irradiation resistance of nanoporous Au through temperature-jump tests. *Acta Mater.* **2018**, *143*, 30–42. [CrossRef]
22. Ma, Y.; Li, H.; Bridges, D.; Peng, P.; Lawrie, B.; Feng, Z.; Hu, A. Zero-dimensional to three-dimensional nanojoining: Current status and potential applications. *RSC Adv.* **2016**, *6*, 75916–75936. [CrossRef]
23. Peng, P.; Liu, L.; Gerlich, A.P.; Hu, A.; Zhou, Y.N. Self-Oriented Nanojoining of Silver Nanowires via Surface Selective Activation. *Part. Part. Syst. Charact.* **2013**, *30*, 420–426. [CrossRef]
24. Al-Hartomy, O.A.; Ibrahim, M.A.; Al-Ghamdi, A.; Dishovsky, N.; Ivanov, M.; Mihaylov, M.; El-Tantawy, F. Dynamic mechanical thermal analysis and dielectric thermal analysis of siloxane rubber-based composites filled with carbon black. *J. Compos. Mater.* **2012**, *46*, 1765–1770. [CrossRef]
25. El Shafee, E.; El Gamal, M.; Isa, M. Electrical properties of multi walled carbon nanotubes/poly(vinylidene fluoride/trifluoroethylene) nanocomposites. *J. Polym. Res.* **2011**, *19*, 9805. [CrossRef]
26. Liang, X.; Zhao, T.; Hu, Y.; Sun, R. Dielectric properties of silver nanowires-filled polyvinylidene fluoride composite with low percolation threshold. *J. Nanopart. Res.* **2014**, *16*, 2578. [CrossRef]
27. He, L.; Tjong, T.S. Low percolation threshold of graphene/polymer composites prepared by solvothermal reduction of graphene oxide in the polymer solution. *Nanoscale Res. Lett.* **2013**, *8*, 132. [CrossRef] [PubMed]
28. Park, J.-Y.; Jung, Y.-S.; Cho, J.; Choi, W.-K. Chemical reaction of sputtered Cu film with PI modified by low energy reactive atomic beam. *Appl. Surf. Sci.* **2006**, *252*, 5877–5891. [CrossRef]
29. Jianfeng, Y.; Guisheng, Z.; Anming, H.; Zhou, Y.N. Preparation of PVP coated Cu NPs and the application for low-temperature bonding. *J. Mater. Chem.* **2011**, *21*, 15981. [CrossRef]
30. Maekawa, K.; Yamasaki, K.; Niizeki, T.; Mita, M.; Matsuba, Y.; Terada, N.; Saito, H. Drop-on-Demand Laser Sintering With Silver Nanoparticles for Electronics Packaging. *IEEE Trans. Compon. Packag. Manuf. Technol.* **2012**, *2*, 868–877. [CrossRef]
31. Peng, P.; Hu, A.; Gerlich, A.P.; Zou, G.; Liu, L.; Zhou, Y.N. Joining of Silver Nanomaterials at Low Temperatures: Processes, Properties, and Applications. *ACS Appl. Mater. Interfaces* **2015**, *7*, 12597–12618. [CrossRef] [PubMed]
32. Peng, P.; Li, L.; Guo, W.; Hui, Z.; Fu, J.; Jin, C.; Liu, Y.; Zhu, Y. Room-Temperature Joining of Silver Nanoparticles Using Potassium Chloride Solution for Flexible Electrode Application. *J. Phys. Chem. C* **2018**, *122*, 2704–2711. [CrossRef]
33. Hui, Z.; Liu, Y.; Guo, W.; Li, L.; Mu, N.; Jin, C.; Zhu, Y.; Peng, P. Chemical sintering of direct-written silver nanowire flexible electrodes under room temperature. *Nanotechnology* **2017**, *28*, 285703. [CrossRef] [PubMed]
34. Guo, W.; Zeng, Z.; Zhang, X.; Peng, P.; Tang, S. Low-Temperature Sintering Bonding Using Silver Nanoparticle Paste for Electronics Packaging. *J. Nanomater.* **2015**, *2015*, 1–7. [CrossRef]
35. Garnett, E.C.; Cai, W.; Cha, J.J.; Mahmood, F.; Connor, S.T.; Greyson Christoforo, M.; Cui, Y.; McGehee, M.D.; Brongersma, M.L. Self-limited plasmonic welding of silver nanowire junctions. *Nat. Mater.* **2012**, *11*, 241–249. [CrossRef] [PubMed]
36. Beresna, M.; Gecevičius, M.; Kazansky, P.G. Ultrafast laser direct writing and nanostructuring in transparent materials. *Adv. Opt. Photonics* **2014**, *6*, 293. [CrossRef]

37. Meschi Amoli, B.; Trinidad, J.; Hu, A.; Zhou, Y.N.; Zhao, B. Highly electrically conductive adhesives using silver nanoparticle (Ag NP)-decorated graphene: The effect of NPs sintering on the electrical conductivity improvement. *J. Mater. Sci. Mater. Electron.* **2014**, *26*, 590–600. [CrossRef]
38. Holmes, A.S.; Khan, A.; Meunier, M.; Rasmussen, N.; Marinov, V.; Arnold, C.B.; Niino, H.; Swenson, O.F.; Geohegan, D.B.; Träger, F.; et al. Laser sintering of direct write silver nano-ink conductors for microelectronic applications. *Photon Process. Microelectron. Photonics VII* **2008**, *6879*, 687910. [CrossRef]
39. Amoli, B.M.; Marzbanrad, E.; Hu, A.; Zhou, Y.N.; Zhao, B. Electrical Conductive Adhesives Enhanced with High-Aspect-Ratio Silver Nanobelts. *Macromol. Mater. Eng.* **2014**, *299*, 739–747. [CrossRef]
40. Zhang, Y.; Liu, S.; Wang, L.; Qin, X.; Tian, J.; Lu, W.; Chang, G.; Sun, X. One-pot green synthesis of Ag nanoparticles-graphene nanocomposites and their applications in SERS, H_2O_2, and glucose sensing. *RSC Adv.* **2012**, *2*, 538–545. [CrossRef]
41. Velo-Gala, I.; López-Peñalver, J.J.; Sánchez-Polo, M.; Rivera-Utrilla, J. Activated carbon as photocatalyst of reactions in aqueous phase. *Appl. Catal. B Environ.* **2013**, *142–143*, 694–704. [CrossRef]
42. Meschi Amoli, B.; Hu, A.; Zhou, N.Y.; Zhao, B. Recent progresses on hybrid micro–nano filler systems for electrically conductive adhesives (ECAs) applications. *J. Mater. Sci. Mater. Electron.* **2015**, *26*, 4730–4745. [CrossRef]
43. Amjadi, M.; Kyung, K.-U.; Park, I.; Sitti, M. Stretchable, Skin-Mountable, and Wearable Strain Sensors and Their Potential Applications: A Review. *Adv. Funct. Mater.* **2016**, *26*, 1678–1698. [CrossRef]